

Encoding Robustness to Image Style via Adversarial Feature Perturbations

Manli Shu¹ Zuxuan Wu² Micah Goldblum³ Tom Goldstein¹

¹ University of Maryland, College Park, USA

² Fudan University, Shanghai, China

³ New York University, New York, USA

manlis@cs.umd.edu, zxwu@fudan.edu.cn, goldblum@nyu.edu, tomg@cs.umd.edu

Abstract

Adversarial training is the industry standard for producing models that are robust to small adversarial perturbations. However, machine learning practitioners need models that are robust to other kinds of changes that occur naturally, such as changes in the style or illumination of input images. Such changes in input distribution have been effectively modeled as shifts in the mean and variance of deep image features. We adapt adversarial training by directly perturbing feature statistics, rather than image pixels, to produce models that are robust to various unseen distributional shifts. We explore the relationship between these perturbations and distributional shifts by visualizing adversarial features. Our proposed method, Adversarial Batch Normalization (AdvBN), is a single network layer that generates worst-case feature perturbations during training. By fine-tuning neural networks on adversarial feature distributions, we observe improved robustness of networks to various unseen distributional shifts, including style variations and image corruptions. In addition, we show that our proposed adversarial feature perturbation can be complementary to existing image space data augmentation methods, leading to improved performance. The source code and pre-trained models are released at <https://github.com/azshue/AdvBN>.

1 Introduction

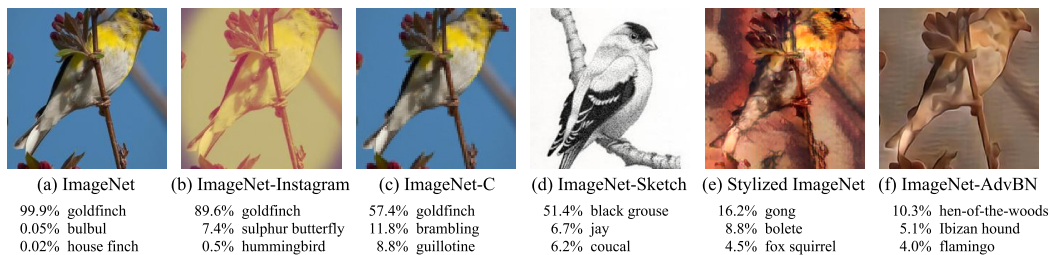


Figure 1: **Images from ImageNet variants along with classification scores by a pre-trained ResNet-50.** The image of column (a) is from ImageNet validation set. Dataset of column (d) is collected independently of the ImageNet dataset. Dataset of Column (f) is generated by our Adversarial Batch Normalization module. Details on how we generate column (f) can be found in Section 3.

Robust optimization for neural networks has been a major focus of recent research. A mainstream approach to reducing the brittleness of classifiers is *adversarial training*, which solves a min-max

optimization problem in which an adversary makes perturbations to images to degrade network performance, while the network adapts its parameters to resist degradation [9, 18, 25]. The result is a hardened network that is no longer brittle to small perturbations to input pixels. While adversarial training makes networks robust to adversarial perturbations, it does not address other forms of brittleness that plague vision systems. For example, shifts in image style, lighting, color mapping, and domain shifts can still severely degrade the performance of neural networks [12].

We propose adapting adversarial training to make neural networks robust to changes in image style and appearance, rather than small perturbations at the pixel level. We formulate a min-max game in which an adversary chooses *adversarial feature statistics*, and network parameters are then updated to resist these changes in feature space that correspond to appearance differences of input images. This game is played until the network is robust to a variety of changes in image space including texture, color, brightness, *etc.*

The idea of adversarial feature statistics is inspired by the observation that the mean and variance of feature maps encode style information, and thus enable the transfer of style information from a source image to a target image through normalization [15, 40]. Unlike standard approaches that rely on feature statistics from auxiliary images to define an image style, we use adversarial optimization of feature statistics to prepare classifiers for the worst-case style that they might encounter.

We propose training with *Adversarial Batch Normalization* (AdvBN) layers. Before each gradient update, the AdvBN layer performs an adversarial feature shift by re-normalizing with the most damaging mean and variance. By using this layer in a robust optimization framework, we create networks that are resistant to various domain shifts representable by shifts in feature statistics. An advantage of this method is that it does not require additional auxiliary data from new domains. We show that robust training with AdvBN layer hardens classifiers against changes in image appearance and style [6, 45], as well as common image corruptions [12]. Besides classification, the effectiveness of AdvBN is also shown in the task of semantic segmentation, where it improves cross-domain generalization.

2 Related work

Adversarial training. Adversarial training and its variants [7, 25, 32, 49] have been widely studied for producing models that are robust to adversarial examples [26, 36] through solving min-max optimization problems. Besides defending against adversarial attacks, recent work has shown that adversarial training can be effectively applied to many other tasks [8, 17, 30, 53, 55]. Adversarial data augmentation [34, 42, 54] proposes to generate worst-case unseen domains using data augmentation and an adversarial loss, thus improving the generalization of neural networks. Another work [46] interprets the original formula of adversarial training as a type of data augmentation and reveals the distributional discrepancy between the feature representations of adversarial examples and clean data. The combination of adversarial training and feature statistics has been studied in previous work [24, 27], where it has been used to defend against adversarial attacks [27], or to generate feature distributions [24]. Our method differs from previous work in both the target of perturbation and the objective function. We craft adversarial feature distributions by directly perturbing the mean and variance of feature maps instead of through a variational auto-encoder [24], and our objective does not include regularization terms.

Feature Perturbation. Feature perturbation has been an effective approach to generate novel data distributions from a given source domain [14, 19, 22, 39]. Feature perturbations can be applied in different ways, such as adding spatial noise to the feature maps [37] or transforming feature maps using classical signal processing [22]. We will specifically discuss feature perturbation through re-normalization. While feature normalization [16, 40] is first proposed to accelerate neural network training [1], the mean and variance of deep feature representations have been shown to effectively capture image style information, and style transfer can be realized through feature re-normalization [15]. The idea of feature re-normalization has also been adopted to help neural networks adapt from the source domain to a target domain, using feature statistics obtained from the latter [21, 31]. Recent work [20] also proposes to use re-normalization for feature interpolation to improve the generalization capability of neural networks. Instead of re-normalizing features with statistics of other samples or from other domains, we simulate the worst-case scenario, encouraging models to be less sensitive to style information and thus to generalize better to images of varying appearances.

Robustness to distribution shifts. The definition of “distribution shifts” varies from one topic to another. For example, distribution shifts in the meta-learning literature [19, 37] often refer to the discrepancy in discriminatory feature distributions of novel tasks from different domains. Another definition is the subtle difference between training and testing data that are sampled from the same underlying distribution [38, 50]. This work mainly focuses on distribution shifts across image data that amount to major “style” discrepancy, including variations in illumination [6, 45], weather condition [29], and image quality degradation [12]. Various methods have been proposed to produce neural networks that generalize well to this type of distribution shift, including test time training [35], test time adaptation [43], training with noise [30], and novel network architectures [28], etc. Data augmentation is a popular method which is designed to increase the diversity of training data and prevent neural networks from over-fitting. Recent studies in data augmentation have proposed to use novel augmentation operations [6, 13, 48, 51], policy searching [3, 10, 23], and adversarial approaches [17, 42, 55], etc. However, the potency of data augmentation can be limited by the choice of applicable augmentations [2, 5]. Feature space augmentation through feature interpolation [20, 41], on the other hand, is not restricted to the family of image transformations. Our method also works in feature space, but instead of interpolating, we perturb feature statistics adversarially.

3 Adversarial Batch Normalization

We propose *Adversarial Batch Normalization* (AdvBN), a module that adversarially perturbs deep feature distributions such that the features confuse CNN classifiers. We iteratively compute adversarial directions in feature space by taking PGD steps on batch statistics. In the next section, we will train on these perturbed feature distributions in order to produce models robust to domain shifts.

Consider a pre-trained classification network, g , with L layers. We divide g into two parts, $g^{1,l}$ and $g^{l+1,L}$, where $g^{m,n}$ denotes layers m through n . Now, consider a batch of data, x , with corresponding labels, y . Formally, the AdvBN module is defined by

$$\text{BN}_{\text{adv}}^{\delta}(x; g, l, y) = \delta'_{\sigma} \cdot \sigma(f) \cdot \left(\frac{f - \mu(f)}{\sigma(f)} \right) + \delta'_{\mu} \cdot \mu(f), \text{ where } f = g^{1,l}(x), \quad (1)$$

$$(\delta'_{\mu}, \delta'_{\sigma}) = \arg \max_{(\delta_{\mu}, \delta_{\sigma})} \mathcal{L} \left[g^{l+1,L} \left(\delta_{\sigma} \cdot (f - \mu(f)) + \delta_{\mu} \cdot \mu(f) \right), y \right], \quad (2)$$

$$\text{subject to } \|\delta_{\mu} - 1\|_{\infty} \leq \epsilon, \|\delta_{\sigma} - 1\|_{\infty} \leq \epsilon,$$

where \mathcal{L} is the cross-entropy loss, and the maximization problem is solved with projected gradient descent. Note that the feature input of $g^{l+1,L}$ is a simplified form of the AdvBN formulation in Eq (1), where the two $\sigma(f)$'s cancel out. Simply put, the AdvBN module is a PGD attack on batch norm statistics which can be inserted inside a network. $\delta_{\mu}, \delta_{\sigma}$ are vectors with length equal to the number of channels in the output of layer l , and we multiply by them entry-wise, one scalar entry per channel, similarly to Batch Normalization. Additionally, note that this module acts on a per-batch basis so that features corresponding to the same image are perturbed differently across training epochs as training samples are randomly shuffled between epochs during training.

In Eq (1), we re-normalize the feature by adding adversarial statistics $\delta_{\mu} \cdot \mu(f)$, rather than simply δ_{μ} , so that ℓ_{∞} bounds and steps size do not need to depend on $\mu(f)$. Intuitively, we permit the mean of adversarial features to vary more when the clean features have a mean of higher magnitude.

Visualizing feature shifts. We adopt the VGG [33] based autoencoder from AdaIN [15], in which the encoder is the first few layers of a pre-trained VGG-19 image classification network. The decoder is trained to restore the input image from the output of the encoder. After we obtain an autoencoder that can perform the identity mapping on input images, we plug in an AdvBN module after the encoder. To compute cross-entropy loss for the AdvBN module, the remaining downstream layers of the aforementioned VGG-19 classifier are used, which takes the encoded feature as input and outputs the class prediction. The features perturbed by AdvBN are then fed into the decoder to create our visualizations.

In Figure 2, images with adversarial feature distributions exhibit differences in color, texture, and edges. We draw two major conclusions from these visualizations which highlight the adversarial properties of these domains. The first one concerns textures: CNNs have been shown to rely heavily

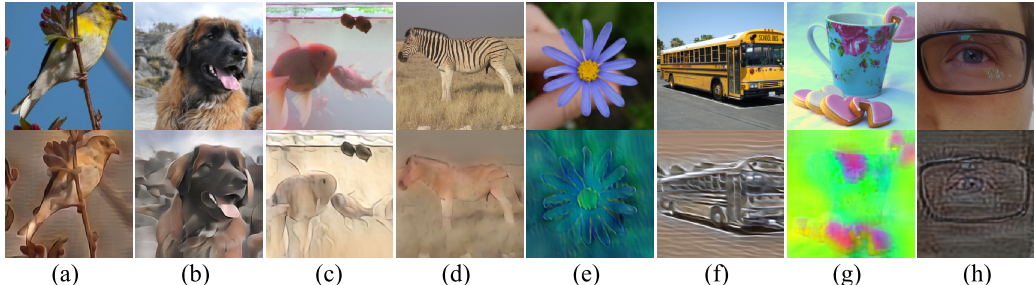


Figure 2: Examples of ImageNet images with adversarial feature distributions shifted by AdvBN, visualized through a decoder. For each pair, the original image is on the top.

on image textures for classification [6]. Images from the adversarial domain, on the other hand, have inconsistent textures across samples. For example, the furry texture of a dog is smoothed in Figure 2 (b), and the stripes disappear from a zebra in Figure 2 (d), whereas visible textures appear in (f) and (g) of Figure 2. The second conclusion pertains to color. Previous study [52] suggests that colors serve as important information for CNNs. In the adversarial domain, we find suppressed colors (Figure 2 (a), (c)) and unnatural hue (Figure 2 (e), (g)). Figure 3 illustrates how the appearance of reconstructed images shifts as adversarial perturbations to feature statistics become larger. See Appendix B for additional examples.

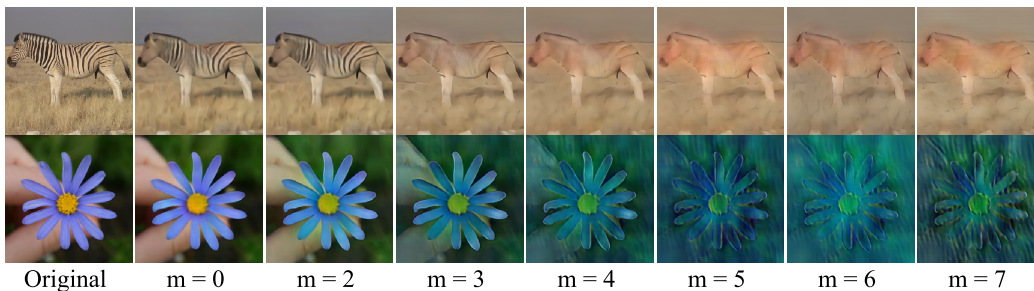


Figure 3: The effect of adversarial strength on visualized examples. m denotes the number of PGD steps. $m = 0$ corresponds to images reconstructed by our autoencoder without AdvBN.

We use this visualization technique to process the entire ImageNet validation set and denote it as ImageNet-AdvBN in Figure 1. By evaluating different methods on this dataset, we observe that performance on ImageNet-AdvBN is consistently degraded, which validates the adversarial property of features generated by AdvBN. Experiments concerning performance on ImageNet-AdvBN are listed in Appendix B.

4 Training with Adversarial Batch Normalization

In this section, we use the proposed AdvBN module to train networks on the perturbed features. The goal is to produce networks that generalize well to unseen domains while maintaining performance on the training distribution, all without having to obtain auxiliary data from new domains.

We start with a pre-trained model, $g = g^{l+1,L} \circ g^{1,l}$, and we fine-tune the subnetwork, $g^{l+1,L}$, on clean and adversarial features simultaneously. To this end, we solve the following min-max problem,

$$\min_{\theta} \mathbb{E}_{(x,y) \sim \mathcal{D}} \left[\max_{\delta} \mathcal{L}(g_{\theta}^{l+1,L} \circ \text{BN}_{\text{adv}}^{\delta} \circ g^{1,l}(x), y) + \mathcal{L}(g_{\theta}^{l+1,L} \circ g^{1,l}(x), y) \right], \quad (3)$$

where \mathcal{L} denotes cross-entropy loss, and \mathcal{D} is the distribution of batches of size n . In order to maintain the network's performance on natural images, we adopt a similar approach to Xie et al. [46] by using auxiliary batch normalization in $g^{l+1,L}$ for adversarial features; we use the original BNs when propagating clean features, and we use auxiliary ones for adversarial features. See Algorithm 1 for a detailed description of our method.

Since we start with pre-trained models, we only need to fine-tune for 20 epochs, yielding improved robustness with little additional computation. Moreover, we only modify the parameters of later layers, so we do not need to backpropagate through the first half of the network. See Appendix C for an analysis of the training budget using our method. In the following section, we measure the performance, on several datasets, of our model fine-tuned using adversarial training with AdvBN.

Algorithm 1: Training with Adversarial Batch Normalization

Input: Training data, pretrained network $g = g_{\theta}^{l+1,L} \circ g^{1,l}$, learning rate α , PGD bound ϵ , and PGD step size τ , loss function \mathcal{L}

Result: Updated network parameters, θ , of subnetwork $g_{\theta}^{l+1,L}$

```

for each training step do
  Sample mini-batch  $x$  with label  $y$ ;
  Obtain feature map  $f = g^{1,l}(x)$ ;
  Initialize perturbation:  $\delta = (\delta_{\mu}, \delta_{\sigma})$ ;
  Let  $f_{adv} = f$ ;
  for adversarial step = 1, ...,  $m$  do
     $f_{adv} \leftarrow \delta_{\sigma} \cdot (f - \mu(f)) + \delta_{\mu} \cdot \mu(f)$ ;
    Update  $\delta$ :
     $\delta \leftarrow \delta + \tau \cdot \text{sign}(\nabla_{\delta} \mathcal{L}(g_{\theta}^{l+1,L}(f_{adv}), y))$ ;
     $\delta \leftarrow \text{clip}(\delta, 1 - \epsilon, 1 + \epsilon)$ ;
  end
   $f_{adv} \leftarrow \delta_{\sigma} \cdot (f - \mu(f)) + \delta_{\mu} \cdot \mu(f)$ ;
  Update  $\theta$  using gradient descent:
   $\theta \leftarrow \theta - \alpha \cdot \nabla_{\theta} \mathcal{L}(g_{\theta}^{l+1,L}(f_{adv}), y) + \mathcal{L}(g_{\theta}^{l+1,L}(f), y)$ ;
end
return  $\theta$ 

```

5 Experiments

In section 5.1, we evaluate our method on image classification. We measure the generalization of models on ImageNet variant datasets that features different distributional shifts. We provide ablation studies of our method in Section 5.2. A feature divergence analysis is presented in Section 5.3 that validates the effectiveness of our method from a different perspective. In section 5.4, we evaluate our method on semantic segmentation. We conduct cross-domain evaluations on traffic scene datasets with different weather conditions and traffic scenes.

5.1 Evaluation on ImageNet Variants

In this section, we evaluate our method in the context of image classification on ImageNet variant datasets. We first evaluate the standalone performance of our method. We also include other baseline methods, including image space adversarial training adapted from the standard PGD adversarial training [25]. MoEx [20] is another related method that performs feature space augmentation through feature re-normalization. SIN [6] is trained on both Stylized ImageNet and original ImageNet, which uses AdaIN [15] as the style transfer method.

In addition, we examine AdvBN as a feature space augmentation method by showing its potential to be complementary to image space augmentation. We consider state-of-the-art data augmentation methods, including AutoAugment[3], Fast AutoAugment (AA)[23], CutMix[48], AugMix[13] and AdvProp[46]. We show that our method can further improve the generalization of models trained with advanced data augmentations. Results of all methods included in this section are based on the ResNet-50 model architecture. Our method also works well on other architectures, and we provide results in Appendix A.

Implementation details. Our model begins with an ImageNet pre-trained ResNet-50 [11]. We insert the AdvBN module at the end of the 2nd convolutional stage (conv2_3). We then fine-tune the model with our method following Algorithm 1 for 20 epochs. The learning rate starts at 0.001 and decreases by a factor of 10 after 10 epochs. Our batch size is set to 256. We use SGD with a momentum of 0.9 and weight decay coefficient 10^{-4} . We search for the optimal number of adversarial

steps m by increasing m while fixing the step size to be $\tau = 0.2$, and we bound the perturbation with $\epsilon = m \cdot \tau - 0.1$. The optimal m we find through this procedure is $m = 6$. When using AdvBN to improve a given data augmentation method, we apply this fine-tuning procedure on a model trained with the data augmentation, except for AA. Due to the absence of a pre-trained AA model, we manage to fine-tune a base model jointly with a fixed AA policy and AdvBN, and we compare it to a model solely fine-tuned with AA. All models trained with AdvBN that appeared in this subsection are obtained by following the same training routine and hyperparameter settings that we specified above.

Datasets. To measure the generalization ability of image classification models, we evaluate our models on four variants of ImageNet [4]:

- **ImageNet-C** [12] (under the Apache License 2.0) contains distorted images with 15 categories of common image corruption applied, each with 5 levels of severity. Performance on this dataset is measured by mean Corruption Error (mCE), the average classification error over a total of 75 combinations of corruption type and severity level, weighted by their difficulty.
- **ImageNet-Instagram (ImageNet-Ins.)** [45] is composed of ImageNet images processed with a total of 20 different Instagram aesthetic image filters. Filters are applied separately, and the dataset contains 20 sub-datasets, each corresponding to one type of image filter.
- **ImageNet-Sketch** [44] (under the MIT License) is a dataset of black and white sketches. The dataset includes 50,000 images in total, falling into 1,000 ImageNet categories, with 50 images per category. Images in this dataset are collected independently from the original ImageNet validation set through Google Image queries. Details concerning the construction of this dataset can be found in Section 4.4 of Wang et al. [44].
- **Stylized ImageNet (ImageNet-Style)** [6] (under the MIT License) consists of images from the ImageNet dataset, each stylized using AdaIN [15] with a randomly selected painting. Textures and colors of images in this dataset differ heavily from the originals.

Table 1: **Evaluation on ImageNet variants.** All methods are implemented based on ResNet-50. Performance on ImageNet-C is measured by mean Corrupted Error (mCE)[13].

Method	ImageNet-C mCE ↓	ImageNet-Ins. Top-1 acc. ↑	ImageNet-Sketch.. Top-1 acc.↑	ImageNet-Style Top-1 acc.↑
Standard Training	76.7	67.2	24.1	7.4
Adv. Training	73.7	68.2	25.3	9.1
MoEx (w/ Cutmix)	74.8	70.0	24.0	5.0
SIN	73.8	68.5	26.9	10.4
AdvBN	72.7	69.5	27.9	11.9
AdvProp	70.7	69.2	18.0	9.0
AdvProp + AdvBN	69.5	69.3	28.7	12.6
Cutmix	74.7	70.3	23.8	5.3
Cutmix + AdvBN	72.1	70.9	27.2	8.2
AutoAugment*(AA)	72.1	70.1	26.7	8.2
AA + AdvBN	68.6	71.1	30.3	14.1
Fast AA	68.7	71.1	27.2	8.3
Fast AA + AdvBN	68.7	71.3	28.6	11.4
Augmix	68.4	70.4	28.5	11.2
Augmix + AdvBN	64.6	71.1	28.7	13.6

Model details. Models trained using other methods that we include in this section are ResNet-50 models released by the authors of the original work, except for methods of which an official ResNet-50 is not available. The released MoEx model is trained collaboratively with CutMix. The “Adv. Training” baseline is adapted from PGD adversarial training, for which we adopt auxiliary batch normalization to alleviate the performance degradation on non-adversarial images, and the model is obtained through fine-tuning on a standard trained model. AdvProp does not provide a ResNet-50 model, and we use the open source implementation¹, and our reproduced model matches the accuracy reported in the aforementioned implementation. Our reported performance using AA, denoted as

¹<https://github.com/tingxueronghua/pytorch-classification-advprop> (MIT License)

“AA*”, is obtained through fine-tuning a pre-trained base model for the same number of epochs as AdvBN, using a fixed set of augmentation operations found by AA, which is included as a reference to the performance of “AdvBN + AA”. The augmentation policy that we use is from the original work and can be found in the open source implementation².

Results. In Table 1, we evaluate the performance of models on the four variant datasets. The standalone AdvBN improves the generalization of a standard model on every dataset and is competitive with alternative methods. Additionally, we find that our method is complementary to input space data augmentation, consistently boosting the performance of state-of-the-art data augmentation methods. Note that our model has auxiliary BN layers, so its performance on the original ImageNet is well maintained, as will be shown in the next subsection. Details concerning inference are in Appendix A.

5.2 Ablation Study

Where should the AdvBN module be placed within a network? The proposed AdvBN module can be inserted after any layer in a network. In this section, we try AdvBN after other layers, namely conv3_4 and conv4_6. For the ablation study, all of our models are obtained by following the same fine-tuning setting found in subsection 5.1, but with a fixed AutoAugment policy as data augmentation. In Table 2, we observe that conv4_6 yields the worst performance among all three ImageNet variants, indicating that using AdvBN at such deep layer is not as helpful as at shallower layers. We hypothesize two possible explanations for this phenomenon: (1) there are fewer trainable parameters when only very deep layers are fine-tuned; (2) features are more abstract at deeper layers, and perturbing these high-level features can lead to extremely chaotic feature representations that are harmful for classification.

Table 2: **Ablation studies on the positioning of AdvBN.** The base model is ResNet-50.

Model	ImageNet top1 acc. \uparrow	ImageNet-C mCE. \downarrow	ImageNet-Ins. top1 acc. \uparrow	ImageNet-Sketch. top1 acc. \uparrow	ImageNet-Style top1 acc. \uparrow
Base model	76.1	76.7	67.2	24.1	7.4
$l = \text{conv2_3}$	76.5	68.6	71.1	30.3	14.1
$l = \text{conv3_4}$	76.2	70.0	70.2	33.2	19.5
$l = \text{conv4_6}$	75.3	75.0	68.5	26.1	11.0

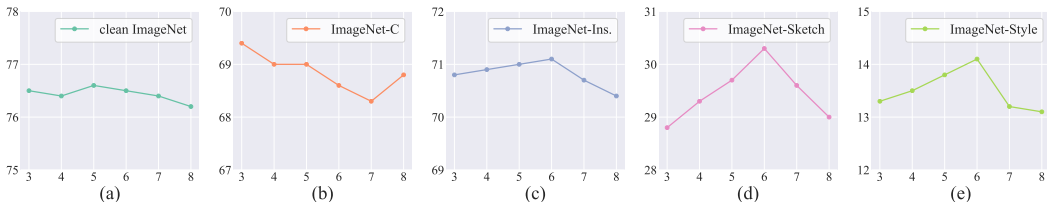


Figure 4: **The effects of adversarial strength.** The y-axis of (b) ImageNet-C is the mean Corrupted Error (mCE), and the others are top-1 accuracies. X-axes are the number of PGD steps m .

Adversarial strength. The strength of the adversarial attack in the adversarial training framework has a major impact on model performance [25]. We test a range of PGD parameters to demonstrate how the strength of AdvBN affects model performance. We measure strength by the perturbation number of PGD steps m , where we fix τ to be 0.2 for all settings and fix the perturbation bound $\epsilon = [m \cdot \tau] - 0.1$ for different m 's.

Results concerning the impact of adversarial strength are shown in Figure 4. We can see that the clean accuracy on ImageNet decreases as the number of steps m grows. On the other datasets, we can observe a turning point, where the performance reaches optimality. This behavior is expected because small perturbations cause small changes to features which may help maintain the clean accuracy but cannot help improve a model’s generalization to other domains; overly large perturbations are also less beneficial as the resulting features can be too noisy.

²<https://github.com/DeepVoltaire/AutoAugment> (MIT License)

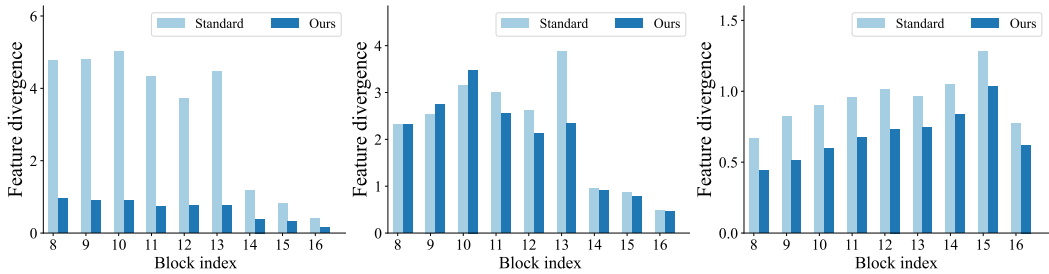
5.3 Feature Divergence Analysis

We compare the features extracted by our network to those of a standard ResNet-50 trained on ImageNet. Following Pan et al. [28], we model features from each channel using a normal distribution with the same mean and standard deviation, and we compute the symmetric KL divergence between the corresponding distributions on the two datasets (A and B). For two sets of deep features, F_A and F_B , each with C channels, the divergence $D(F_A||F_B)$ is computed using the formula,

$$D(F_A||F_B) = \frac{1}{C} \sum_{i=1}^C (KL(F_A^i||F_B^i) + KL(F_B^i||F_A^i)), \quad (4)$$

$$KL(F_A^i||F_B^i) = \log \frac{\sigma_B^i}{\sigma_A^i} + \frac{\sigma_A^{i2} + (\mu_A^i - \mu_B^i)^2}{2\sigma_B^{i2}} - \frac{1}{2}, \quad (5)$$

where F^i denotes the features of i -th channel with mean μ^i and standard deviation σ^i .



(a) ImageNet vs. ImageNet-Ins. (b) ImageNet vs. ImageNet-Sketch (c) ImageNet vs. ImageNet-Style

Figure 5: **Feature divergence between pairs of datasets.** Features are extracted by a standard and an AdvBN fine-tuned ResNet50.

In Figure 5, we compare the baseline model with our own on three pairs of datasets in the fine-tuned layers. Since ImageNet-Instagram contains 20 filter versions, we use the “Toaster” filter found in [45] to cause the sharpest drop in classification performance.

Feature divergence in our network trained with AdvBN is substantially smaller in the deeper layers of the fine-tuned subnetwork. In other words, the distribution of deep features corresponding to shifted domains is very similar to the distribution of deep features corresponding to standard ImageNet data. The small divergence between feature representations explains the effectiveness of AdvBN from a different angle and explains why our model generalizes well across datasets.

5.4 Generalization on Semantic Segmentation

Datasets. We present domain generalization results on the Synthia video sequences dataset³ [29], consisting of multiple sub-datasets featuring traffic situations under different weather, illumination, and season conditions. We conduct experiment on 10 sub-datasets that include two different road scenes: “Highway” and “New York-like City”, each one with 5 different domain shifted variants: “dawn”, “fog”, “night”, “spring” and “winter”. Figure 6 shows sample images from each of the 10 sub-datasets. We use the left-front view images of each sub-dataset, and split dataset by randomly selecting 900 images for training and 500 for validation. We separately train two sets of models on the “Highway/ Dawn” and “New York-like City/ Spring” datasets and evaluate them on all the 10 sub-datasets within the two road scenes.

Implementation details. The segmentation model we use is a ResNet-50 based segmentation network with dilated convolutions [47]. Our baseline models are trained for 80 epochs following the training protocol from [28]. We apply AdvBN by placing it after layer conv2_3 of the baseline model and fine-tuning on a given sub-dataset for 30 epochs, with adversarial training parameters $\tau = 0.2$, $\epsilon = 0.5$, and 3 repeats.

³<http://synthia-dataset.net/>, subject to Attribution-NonCommercial-ShareAlike 3.0.



Figure 6: **Example images from the Synthia video sequences dataset.** The top row contains traffic scenes of the “Highway” subset, and the bottom row is the “New York-like City”.

Table 3: **Segmentation results on the Synthia dataset.** Evaluation metric is mean IoU (Intersection over Union). The first column denotes the dataset used for training.

		New York-like City					Highway				
		Dawn	Fog	Night	Spring	Winter	Dawn	Fog	Night	Spring	Winter
NY.Like C./ Spring	baseline	52.7	49.5	49.7	65.9	48.2	18.6	21.0	16.9	21.6	15.3
	+ Adv. Training	54.6	50.7	50.2	65.8	49.7	21.2	28.0	20.4	26.3	21.4
	AdvProp	52.3	48.9	48.0	71.9	48.2	18.9	22.0	13.8	24.3	17.5
	MoEx	54.7	53.2	51.8	71.1	49.0	21.3	24.3	19.4	27.6	18.7
	+ AdvBN	57.5	55.1	55.4	66.5	52.7	23.8	26.6	25.9	29.8	23.5
Highway/ Dawn	baseline	32.6	29.0	25.4	24.2	24.8	64.2	55.5	53.1	59.0	49.2
	+ Adv. Training	33.5	30.7	27.9	27.5	26.7	64.0	56.4	54.0	59.5	50.3
	AdvProp	30.8	24.1	20.3	23.2	21.4	64.6	53.5	47.2	59.0	47.6
	MoEx	32.0	27.5	27.6	29.6	26.7	64.6	57.2	57.0	61.0	51.1
	+ AdvBN	34.0	31.6	29.6	30.7	29.1	64.5	57.2	56.4	61.2	53.2

We also include the results of several alternative methods from Section 5.1. For the image space adversarial training, we adopt the same training settings as we do for AdvBN, except for the adversarial training parameters (perturbation size and bound). We find the optimal perturbation size for adversarial training through grid search and report the best results. The optimal hyperparameters we find are $\tau = 1$, $\epsilon = 1$. Auxiliary BNs are not used for either method at inference time. For MoEx and AdvProp, we train them for 110 epochs to match the number of optimization steps with our AdvBN fine-tuned model. Note that we do not include other data augmentation methods from Section 5.1 because they are originally designed for the image classification problems, which include operations that can be tricky to be applied to dense prediction problems like semantic segmentation.

We evaluate the performance of semantic segmentation using the mean IoU (Intersection over Union) metric. In table 3, over 20 source-target domain pairs, we show that AdvBN achieves the best cross-domain generalization performance. Our method also improves in-domain performance over standard training, while AdvProp achieves the highest performance under in-domain settings. Results in this section are consistent with our observation on image classification in Section 5.1.

6 Conclusion and Discussion

Our work studies how perturbing feature statistics simulate distribution shifts in image data. We find that fine-tuning on images with adversarially shifted feature distributions improves a model’s robustness towards various domain shifts without using auxiliary data. As AdvBN operates purely in feature space, it is complementary to existing input space data augmentation methods, and can further improve the generalization of state-of-the-art methods. Future work will be to adapt our method to tasks beyond vision. It is known that adversarial perturbations in input space boost performance for language [55] and graph [17] models, and these data modalities may benefit from more structured feature-space perturbations.

Limitations and Impact. While AdvBN can offer impactful improvements for domain generalization, it may in some cases trade off performance on non-shifted in-distribution testing data. Moreover, real-world datasets and distributional shifts vary dramatically, and practitioners should be cautious rather than expecting that the performance seen on benchmark datasets, such as ImageNet variants, will translate to performance boosts in their own settings.

Acknowledgements

Shu and Goldstein were supported by the ONR MURI program, with additional support provided by DARPA GARD. Wu was supported by NSFC under Grant No. 62102092.

References

- [1] Nils Bjorck, Carla P Gomes, Bart Selman, and Kilian Q Weinberger. Understanding batch normalization. In *NIPS*, 2018.
- [2] Ting Chen, Simon Kornblith, Mohammad Norouzi, and Geoffrey E. Hinton. A simple framework for contrastive learning of visual representations. In *ICML*, 2020.
- [3] Ekin D Cubuk, Barret Zoph, Dandelion Mane, Vijay Vasudevan, and Quoc V Le. Autoaugment: Learning augmentation strategies from data. In *CVPR*, 2019.
- [4] J. Deng, W. Dong, R. Socher, L.-J. Li, K. Li, and L. Fei-Fei. ImageNet: A Large-Scale Hierarchical Image Database. In *CVPR09*, 2009.
- [5] Robert Geirhos, Carlos RM Temme, Jonas Rauber, Heiko H Schütt, Matthias Bethge, and Felix A Wichmann. Generalisation in humans and deep neural networks. In *NIPS*, 2018.
- [6] Robert Geirhos, Patricia Rubisch, Claudio Michaelis, Matthias Bethge, Felix A. Wichmann, and Wieland Brendel. Imagenet-trained cnns are biased towards texture; increasing shape bias improves accuracy and robustness. In *ICLR*, 2019.
- [7] Micah Goldblum, Liam Fowl, Soheil Feizi, and Tom Goldstein. Adversarially robust distillation. In *AAAI*, 2020.
- [8] ChengYue Gong, Tongzheng Ren, Mao Ye, and Qiang Liu. Maxup: A simple way to improve generalization of neural network training. *CoRR*, abs/2002.09024, 2020.
- [9] Ian J. Goodfellow, Jonathon Shlens, and Christian Szegedy. Explaining and harnessing adversarial examples. In *ICLR*, 2015.
- [10] Ryuichiro Hataya, Jan Zdenek, Kazuki Yoshizoe, and Hideki Nakayama. Faster autoaugment: Learning augmentation strategies using backpropagation. In *ECCV*, 2020.
- [11] Kaiming He, Xiangyu Zhang, Shaoqing Ren, and Jian Sun. Deep residual learning for image recognition. In *CVPR*, 2016.
- [12] Dan Hendrycks and Thomas G. Dietterich. Benchmarking neural network robustness to common corruptions and perturbations. In *ICLR*, 2019.
- [13] Dan Hendrycks, Norman Mu, Ekin Dogus Cubuk, Barret Zoph, Justin Gilmer, and Balaji Lakshminarayanan. Augmix: A simple data processing method to improve robustness and uncertainty. In *ICLR*, 2020.
- [14] Han-Kai Hsu, Chun-Han Yao, Yi-Hsuan Tsai, Wei-Chih Hung, Hung-Yu Tseng, Maneesh Kumar Singh, and Ming-Hsuan Yang. Progressive domain adaptation for object detection. In *WACV*, 2020.
- [15] Xun Huang and Serge Belongie. Arbitrary style transfer in real-time with adaptive instance normalization. In *ICCV*, 2017.
- [16] Sergey Ioffe and Christian Szegedy. Batch normalization: Accelerating deep network training by reducing internal covariate shift. In *ICML*, 2015.
- [17] Kezhi Kong, Guohao Li, Mucong Ding, Zuxuan Wu, Chen Zhu, Bernard Ghanem, Gavin Taylor, and Tom Goldstein. Flag: Adversarial data augmentation for graph neural networks. *arXiv preprint arXiv:2010.09891*, 2020.
- [18] Alexey Kurakin, Ian J. Goodfellow, and Samy Bengio. Adversarial machine learning at scale. In *ICLR*, 2017.

- [19] Haebeom Lee, Taewook Nam, Eunho Yang, and Sung Ju Hwang. Meta dropout: Learning to perturb latent features for generalization. In *ICLR*, 2020.
- [20] Boyi Li, Felix Wu, Ser-Nam Lim, Serge J. Belongie, and Kilian Q. Weinberger. On feature normalization and data augmentation. In *CVPR*, 2021.
- [21] Yanghao Li, Naiyan Wang, Jianping Shi, Jiaying Liu, and Xiaodi Hou. Revisiting batch normalization for practical domain adaptation. In *ICLR Workshop*, 2017.
- [22] Yijun Li, Chen Fang, Jimei Yang, Zhaowen Wang, Xin Lu, and Ming-Hsuan Yang. Universal style transfer via feature transforms. In *NIPS*, 2017.
- [23] Sungbin Lim, Ildoo Kim, Taesup Kim, Chiheon Kim, and Sungwoong Kim. Fast autoaugment. In *NeurIPS*, 2019.
- [24] Yawei Luo, Ping Liu, Tao Guan, Junqing Yu, and Yi Yang. Adversarial style mining for one-shot unsupervised domain adaptation. In *NeurIPS*, 2020.
- [25] Aleksander Madry, Aleksandar Makelov, Ludwig Schmidt, Dimitris Tsipras, and Adrian Vladu. Towards deep learning models resistant to adversarial attacks. In *ICLR*, 2018.
- [26] Seyed-Mohsen Moosavi-Dezfooli, Alhussein Fawzi, and Pascal Frossard. Deepfool: a simple and accurate method to fool deep neural networks. In *CVPR*, 2016.
- [27] Muzammal Naseer, Salman Khan, Munawar Hayat, Fahad Shahbaz Khan, and Fatih Porikli. Stylized adversarial defense. *CoRR*, abs/2007.14672, 2020.
- [28] Xingang Pan, Ping Luo, Jianping Shi, and Xiaoou Tang. Two at once: Enhancing learning and generalization capacities via ibn-net. In *ECCV*, 2018.
- [29] German Ros, Laura Sellart, Joanna Materzynska, David Vazquez, and Antonio M. Lopez. The synthia dataset: A large collection of synthetic images for semantic segmentation of urban scenes. In *CVPR*, June 2016.
- [30] Evgenia Rusak, Lukas Schott, Roland S. Zimmermann, Julian Bitterwolf, Oliver Bringmann, Matthias Bethge, and Wieland Brendel. A simple way to make neural networks robust against diverse image corruptions. In *ECCV*, 2020.
- [31] Steffen Schneider, Evgenia Rusak, Luisa Eck, Oliver Bringmann, Wieland Brendel, and Matthias Bethge. Improving robustness against common corruptions by covariate shift adaptation. In *NeurIPS*, 2020.
- [32] Ali Shafahi, Mahyar Najibi, Mohammad Amin Ghiasi, Zheng Xu, John Dickerson, Christoph Studer, Larry S Davis, Gavin Taylor, and Tom Goldstein. Adversarial training for free! In *NeurIPS*, 2019.
- [33] Karen Simonyan and Andrew Zisserman. Very deep convolutional networks for large-scale image recognition. In *ICLR*, 2015.
- [34] Aman Sinha, Hongseok Namkoong, and John C. Duchi. Certifying some distributional robustness with principled adversarial training. In *ICLR*, 2018.
- [35] Yu Sun, Xiaolong Wang, Zhuang Liu, John Miller, Alexei A. Efros, and Moritz Hardt. Test-time training with self-supervision for generalization under distribution shifts. In *ICML*, 2020.
- [36] Christian Szegedy, Wojciech Zaremba, Ilya Sutskever, Joan Bruna, Dumitru Erhan, Ian J. Goodfellow, and Rob Fergus. Intriguing properties of neural networks. In *ICLR*, 2014.
- [37] Hung-Yu Tseng, Hsin-Ying Lee, Jia-Bin Huang, and Ming-Hsuan Yang. Cross-domain few-shot classification via learned feature-wise transformation. In *ICLR*, 2020.
- [38] Dimitris Tsipras, Shibani Santurkar, Logan Engstrom, Alexander Turner, and Aleksander Madry. Robustness may be at odds with accuracy. In *ICLR*, 2019.

- [39] Eric Tzeng, Judy Hoffman, Kate Saenko, and Trevor Darrell. Adversarial discriminative domain adaptation. In *CVPR*, 2017.
- [40] Dmitry Ulyanov, Andrea Vedaldi, and Victor S. Lempitsky. Instance normalization: The missing ingredient for fast stylization. *CoRR*, abs/1607.08022, 2016.
- [41] Vikas Verma, Alex Lamb, Christopher Beckham, Amir Najafi, Ioannis Mitliagkas, David Lopez-Paz, and Yoshua Bengio. Manifold mixup: Better representations by interpolating hidden states. In *ICML*, 2019.
- [42] Riccardo Volpi, Hongseok Namkoong, Ozan Sener, John C. Duchi, Vittorio Murino, and Silvio Savarese. Generalizing to unseen domains via adversarial data augmentation. In *NeurIPS*, 2018.
- [43] Dequan Wang, Evan Shelhamer, Shaoteng Liu, Bruno A. Olshausen, and Trevor Darrell. Tent: Fully test-time adaptation by entropy minimization. In *ICLR*, 2021.
- [44] Haohan Wang, Songwei Ge, Zachary Lipton, and Eric P Xing. Learning robust global representations by penalizing local predictive power. In *NeurIPS*, 2019.
- [45] Zhe Wu, Zuxuan Wu, Bharat Singh, and Larry S. Davis. Recognizing instagram filtered images with feature de-stylization. In *AAAI*, 2020.
- [46] Cihang Xie, Mingxing Tan, Boqing Gong, Jiang Wang, Alan L. Yuille, and Quoc V. Le. Adversarial examples improve image recognition. In *CVPR*, 2020.
- [47] Fisher Yu and Vladlen Koltun. Multi-scale context aggregation by dilated convolutions. In *ICLR*, 2016.
- [48] Sangdoon Yun, Dongyoon Han, Seong Joon Oh, Sanghyuk Chun, Junsuk Choe, and Youngjoon Yoo. Cutmix: Regularization strategy to train strong classifiers with localizable features. In *ICCV*, 2019.
- [49] Dinghuai Zhang, Tianyuan Zhang, Yiping Lu, Zhanxing Zhu, and Bin Dong. You only propagate once: Accelerating adversarial training via maximal principle. In *NeurIPS*, 2019.
- [50] Hongyang Zhang, Yaodong Yu, Jiantao Jiao, Eric P. Xing, Laurent El Ghaoui, and Michael I. Jordan. Theoretically principled trade-off between robustness and accuracy. In *ICML*, 2019.
- [51] Hongyi Zhang, Moustapha Cissé, Yann N. Dauphin, and David Lopez-Paz. mixup: Beyond empirical risk minimization. In *ICLR*, 2018.
- [52] Richard Zhang, Phillip Isola, and Alexei A Efros. Colorful image colorization. In *ECCV*, 2016.
- [53] Xinyu Zhang, Qiang Wang, Jian Zhang, and Zhao Zhong. Adversarial autoaugment. In *ICLR*, 2020.
- [54] Long Zhao, Ting Liu, Xi Peng, and Dimitris N. Metaxas. Maximum-entropy adversarial data augmentation for improved generalization and robustness. In *NeurIPS*, 2020.
- [55] Chen Zhu, Yu Cheng, Zhe Gan, Siqi Sun, Tom Goldstein, and Jingjing Liu. Freelb: Enhanced adversarial training for natural language understanding. In *ICLR*, 2020.

A Additional results and experiment details

A.1 Detailed results on ImageNet-C

In this section, we provide a detailed version of the results shown in our experiment section concerning the ImageNet-C dataset, which technically contains a total of 75 variants of the ImageNet dataset. The 75 variants fall into 15 categories of corruption; each category presents 5 gradually increasing degrees of severity, where “degree=1” denotes the lowest degree of severity.

Table 4: mean Corrupted Error (mCE) of each corruption category in ImageNet-C.

Network	Noise					Blur				Weather				Digital				mCE
	Clean	Gauss.	Shot	Impulse		Defocus	Glass	Motion	Zoom	Snow	Frost	Fog	Bright	Contrast	Elastic	Pixel	JPEG	
Base model	23.9	80	82	83		75	89	78	80	78	75	66	57	71	85	77	77	76.7
AdvBN	23.0	75	76	77		70	85	75	80	74	71	63	54	66	82	71	72	72.7

Table 5: Raw error of each subset in ImageNet-C .

Model	Corruption	Degree					Corruption	Degree					Corruption	Degree										
		1	2	3	4	5		1	2	3	4	5		1	2	3	4	5						
AugMix + AdvBN	Blur-Defocus	35	40	50	62	74	Blur-Glass	39	50	74	78	84	Blur-Motion	28	33	42	58	71	Blur-Zoom	38	45	49	57	65
		34	39	51	64	74		38	49	74	79	86		29	36	50	69	80		42	51	57	65	73
AugMix + AdvBN	Weather-Snow	39	59	57	69	77	Weather-Frost	35	50	62	64	71	Weather-Fog	37	42	52	58	75	Weather-Bright	25	26	29	33	40
		40	59	56	68	75		34	49	60	62	69		34	40	48	55	72		24	25	28	32	37
AugMix + AdvBN	Digital-Contrast	29	33	39	59	85	Digital-Elastic	31	53	37	48	71	Digital-Pixel	30	32	41	53	60	Digital-JPEG	32	35	37	43	52
		29	33	41	63	87		31	53	38	50	75		30	31	40	53	58		31	34	36	41	49
AugMix + AdvBN	Noise-Gauss.	32	40	55	76	94	Noise-Shot	33	42	55	77	88	Noise-Impulse	36	46	56	79	95						
		31	37	48	64	84		32	39	49	69	81		37	44	51	67	84						

In Table 4, we list the mCE of each corruption category. The mCE of a given category is calculated by taking the average of the 5 corruption errors corresponding to the 5 corruption degrees of the given category, and then normalize the mean value with a constant. The constant differs between corruption categories, which reflects the difficulty of a given corruption type. For detailed formulations, please refer to the official ImageNet-C repository⁴. From the results, we can see that AdvBN alone can improve the baseline model on all corruption types. In Table 5, we list the raw error rate on each sub-dataset in ImageNet-C. The two models in this table are the AugMix model and AugMix model fine-tuned with AdvBN respectively.

A.2 Other architectures

We apply our method to other network architectures and evaluate on the task of image classification. Datasets in Table 6 are the same as in Table 1. We apply AdvBN using the same setting as introduced in Section 5.1, by fine-tuning a pre-trained model for 20 epochs using SGD optimizer. For DenseNet-121, we place the AdvBN layer after the first block, and we use 6 PGD steps with stepsize $\tau = 0.2$, $\epsilon = 1.1$. For the EfficientNet, we place the AdvBN layer after the second block, and we use 3 PGD steps with stepsize $\tau = 0.2$, $\epsilon = 0.5$.

Table 6: Applying AdvBN to other architectures.

Architecture	ImageNet-C mCE. ↓	ImageNet-Ins. Top-1 acc. ↑	ImageNet-Sketch Top-1 acc. ↑	ImageNet-Style Top-1 acc. ↑
DenseNet-121 + AdvBN (w/ AA)	73.4 70.4	66.6 69.3	24.3 28.6	7.9 15.5
EfficientNet-B0 + AdvBN (w/ AA)	72.1 68.7	69.7 71.3	26.7 27.4	12.5 15.7

⁴<https://github.com/hendrycks/robustness>

A.3 AdvBN at inference time

Models containing Batchnorm layers, such as ResNet, will have two sets of BN statistics in deeper layers after being fine-tuned by our method, because we use auxiliary BN [46] for propagating adversarially perturbed features. The auxiliary BN in our model stores the mean and standard deviation of the adversarial feature, which is very different from the feature statistics of the original data.

Intuitively, when testing on data whose distribution is “close” to the training data, using the main BN (as compared to the auxiliary BN) in a model would be more favorable than using the auxiliary BN, and vice versa. In this work, we take a naive measurement for the “closeness” of an ImageNet variant to the original ImageNet by comparing a model’s accuracy on the two datasets. For example, on ImageNet-Instagram, the accuracy of a standard baseline is not degraded much from that on the original ImageNet validation set, and we consider it to be “close” to the original data. Following this rule, at the inference time, we use the main BN on the original ImageNet, ImageNet-Instagram and ImageNet-C, and use auxiliary BN on ImageNet-Sketch and ImageNet-Style. A future direction is to improve the measurement of the distance between test samples and the training data using unsupervised techniques. To demonstrate the discrepancy of the main and auxiliary BN statistics in our model, we include full results of using both statistics in Table 7.

Table 7: Evaluation using main and auxiliary batch normalization statistics respectively.

Method	ImageNet-C mCE ↓	ImageNet-Ins. Top-1 acc. ↑	ImageNet-Sketch.. Top-1 acc.↑	ImageNet-Style Top-1 acc.↑
Standard Training	76.7	67.2	24.1	7.4
AdvBN (w/ main BN)	72.7	69.5	26.4	9.0
AdvBN (w/ aux. BN)	72.4	68.5	27.9	11.9

B ImageNet-AdvBN Dataset

B.1 Creation of the ImageNet-AdvBN dataset

We process the entire ImageNet validation set using the visualization technique introduced in Section 3. We consider two encoder architectures: one is the VGG-19 encoder we use for visualization, another consists of layers of a ResNet-50 up to conv2_3. Both encoders are paired with the same decoder architecture from Huang and Belongie [15]. The resulting datasets, denoted by ImageNet-AdvBN-VGG and ImageNet-AdvBN-ResNet respectively, contain 50000 images each. The data we synthesize for testing other models is generated using these autoencoders that contain the AdvBN module but on ImageNet validation data. AdvBN is conducted with 6 steps, stepsize = 0.20, $\epsilon = 1.1$, and a batch size of 32. We do not shuffle the ImageNet validation data when generating these batches.

B.2 Classification on ImageNet-AdvBN

Table 8 shows the classification performance of various models on the two ImageNet-AdvBN variants, denoted as IN-Adv-VGG and IN-Adv-ResNet respectively. Models in Table 8 are the same ResNet-50 models we use in section 5.1, where we give the details of each model. The significantly degraded accuracy on our generated dataset indicates the adversarial property of our method. We also test these models on ImageNet images reconstructed using our autoencoders, denoted as VGG Reconstructed and ResNet Reconstructed, for each autoencoder. The performance gap between ImageNet-AdvBN and Reconstructed ImageNet indicates that the degradation on ImageNet-AdvBN is not solely caused by the reconstruction loss due to the autoencoders we use.

B.3 Additional Example Images

We include more images from ImageNet-AdvBN-VGG in this section. Example images in Figure 7 are randomly chosen. We do not include the ImageNet-AdvBN-ResNet, because the resulting images are mostly in extreme contrast with small textures that are hard to observe. It is possible that features output from ResNet based encoders are more sensitive to AdvBN perturbations; another explanation is that the features we extract from ResNet-50 are relatively shallow features compared to their VGG counterparts.

Table 8: **Classification accuracy on ImageNet-AdvBN and reconstructed images.** Models of all methods are implemented based on ResNet-50 and trained on the original ImageNet training set. IN-Adv-VGG and IN-Adv-ResNet are two ImageNet-AdvBN datasets generated using different auto-encoders. VGG-reconstructed and ResNet-reconstructed are two datasets generated using the same auto-encoder as their AdvBN counterparts but without feature perturbation.

Method	ImageNet Top-1 acc. \uparrow	IN-Adv-VGG Top-1/ Top-5 acc. \uparrow	VGG Reconstructed Top-1/ Top-5 acc. \uparrow	IN-Adv-ResNet Top-1/ Top-5 acc. \uparrow	ResNet Reconstructed Top-1/ Top-5 acc. \uparrow
Standard Training	76.1	1.6/ 4.7	45.8/ 70.6	0.4/ 1.3	65.7/ 86.9
MoEx (w/ Cutmix)	79.1	1.0/ 2.9	40.2/ 63.8	0.3/ 1.1	65.7/ 86.8
Adv. Training	76.6	2.0/ 5.5	48.1/ 72.5	0.5/ 1.5	68.0/ 88.3
AdvBN	77.0	4.7/ 11.9	46.8/ 71.4	1.7/ 4.0	67.2/ 87.9
AdvProp	77.4	1.6/ 4.5	53.1/ 76.6	0.3/ 0.9	71.1/ 90.0
AdvProp + AdvBN	77.3	7.4/ 17.2	51.4/ 75.3	1.8/ 4.2	70.5/ 89.7
Cutmix	78.6	1.1/ 3.2	39.0/ 62.2	0.3/ 1.0	64.6/ 85.8
Cutmix + AdvBN	78.4	4.1/ 10.3	42.3/ 66.3	1.4/ 3.4	66.7/ 87.4
AA*	76.4	1.9/ 5.3	45.8/ 70.2	0.8/ 2.3	65.5/ 86.9
AA + AdvBN	76.5	6.3/ 15.6	54.6/ 78.3	2.9/ 6.4	66.4/ 87.3
Fast AA	77.8	1.9/ 5.0	43.4/ 67.0	0.8/ 2.5	66.8/ 87.3
Fast AA + AdvBN	77.6	5.1/ 12.8	44.4/ 68.5	1.8/ 4.4	67.4/ 87.8
AugMix	77.6	3.9/ 9.9	53.5/ 77.0	1.0/ 2.7	71.9/ 90.7
AugMix + AdvBN	77.8	8.6/ 19.5	50.9/ 74.7	2.4/ 5.3	70.2/ 89.7

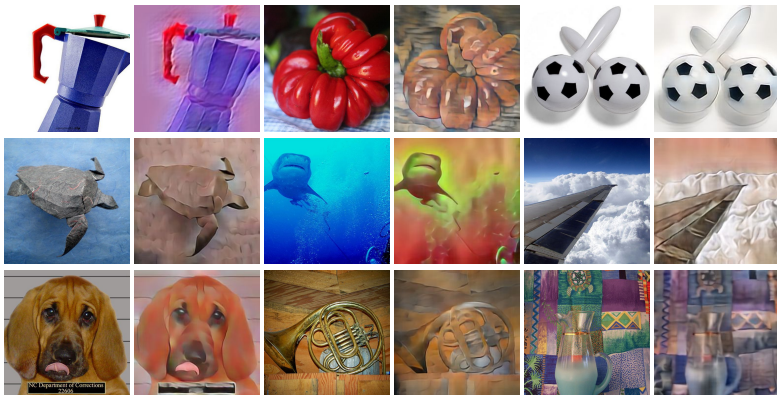


Figure 7: More example images. For each pair of adjacent columns, original versions are on the left, ImageNet-AdvBN-VGG is on the right.

C Details concerning the training budget

We evaluate the training time of our method on a workstation with 4 GeForce RTX 2080 Ti GPUs. We use the default settings for AdvBN on ResNet-50: an AdvBN layer placed after the conv2_3 layer, and 20 epochs of fine-tuning with 6-step PGD inside the AdvBN layer. Fine-tuning is conducted on the ImageNet training set, containing 1.3 million images. Training in this setting takes approximately 48 hours, with batch size set to 256. Besides the model size (i.e., the number of model parameters),

Table 9: **Training duration of AdvBN under different model configurations.** l denotes the placement of the AdvBN layer within a ResNet-50, and m is the number of PGD steps.

Model configuration	$l=\text{conv2_3}$						$l=\text{conv2_3}$	$l=\text{conv3_4}$	$l=\text{conv4_6}$
	$m=3$	$m=4$	$m=5$	$m=6$	$m=7$	$m=8$	$m=6$		
Training duration (hrs)	30	36	43	48	53	59	48	31	15

there are other factors that can affect the training speed of our method. The first factor is the number of PGD steps used by AdvBN layer, as each step evokes a backpropagation through the later part (after the AdvBN layer) of the network. The default setting of our method on ResNet-50 uses 6 PGD steps, so the training time is longer than standard training for the same number of epochs. Another factor is the placement of AdvBN layer within a network. In each PGD step, gradients only backpropagate through the sub-network after the AdvBN layer, so it takes a notably shorter time to train a model with our method, if the AdvBN layer is placed at later network layers.